



## Article

# Forest Age Mapping Using Landsat Time-Series Stacks Data Based on Forest Disturbance and Empirical Relationships between Age and Height

Lei Tian <sup>1</sup> , Longtao Liao <sup>1</sup>, Yu Tao <sup>1,2</sup>, Xiaocan Wu <sup>1</sup> and Mingyang Li <sup>1,\*</sup>

<sup>1</sup> Co-Innovation Center for Sustainable Forestry in Southern China, Nanjing Forestry University, Nanjing 210037, China; tianlei@njfu.edu.cn (L.T.); tao@njfu.edu.cn (L.L.); taoyu@chzu.edu.cn (Y.T.); wuxiaocan@njfu.edu.cn (X.W.)

<sup>2</sup> Anhui Province Key Laboratory of Physical Geographical Environment, Chuzhou 239000, China

\* Correspondence: lmy196727@njfu.edu.cn

**Abstract:** Forest age is a critical parameter for the status and potential of carbon sequestration in forest ecosystems and reflects major forest disturbance information. However, reliable forest age data with high spatial resolution are lacking to date. In this study, we proposed a forest age mapping method with a 30 m resolution that considers forest disturbance. Here, we used the Landsat time-series stacks (LTSS) data from 1986 to 2021 and implemented the LandTrendr algorithm on the Google Earth Engine (GEE) platform to detect the age of disturbed forests. The age of non-disturbed forests was extracted based on forest canopy height data and the empirical relationship between age and height. High-resolution Google images combined with the forest management archive data of forestry departments and national forest inventory (NFI) data were used for the validation of disturbed and non-disturbed forest age, respectively. The results showed that the LandTrendr algorithm detected disturbance years with producer and user accuracies of approximately 94% and 95%, respectively; and the age of non-disturbed forests obtained using the empirical age–height relationship showed an  $R^2$  of 0.8875 and a root mean squared error (RMSE) value of 5.776 with NFI-based results. This confirms the reliability of the proposed 30 m resolution forest age mapping method considering forest disturbance. Overall, the method can be used to produce spatially explicit forest age data with high resolution, which can contribute to the sustainable use of forest resources and enhance the understanding of carbon budget studies in forest ecosystems.

**Keywords:** forest age; LandTrendr; forest disturbance; age and height relationship; Landsat time-series stacks



**Citation:** Tian, L.; Liao, L.; Tao, Y.; Wu, X.; Li, M. Forest Age Mapping Using Landsat Time-Series Stacks Data Based on Forest Disturbance and Empirical Relationships between Age and Height. *Remote Sens.* **2023**, *15*, 2862. <https://doi.org/10.3390/rs15112862>

Academic Editors: Jia Yang, Guangsheng Chen and Zoltan Szantoi

Received: 21 April 2023

Revised: 24 May 2023

Accepted: 30 May 2023

Published: 31 May 2023



**Copyright:** © 2023 by the authors. Licensee MDPI, Basel, Switzerland. This article is an open access article distributed under the terms and conditions of the Creative Commons Attribution (CC BY) license (<https://creativecommons.org/licenses/by/4.0/>).

## 1. Introduction

Forest ecosystems, which account for approximately one third of the Earth's land surface [1], serve as the largest terrestrial carbon pool [2,3]. Forest ecosystems store an estimated 76–98% of terrestrial organic carbon, with about 80% located above ground and 40% below ground, and have contributed to the major carbon sink of terrestrial ecosystems in recent decades [4,5]. Through the process of absorbing greenhouse gases, mainly including carbon dioxide (CO<sub>2</sub>), forest ecosystems play a crucial role in mitigating global climate change by reducing greenhouse gas concentrations, which highlights their critical role in the global carbon cycle [6–13].

The carbon strength (i.e., carbon sinks or sources) of forest ecosystems is influenced by environmental changes, such as CO<sub>2</sub> fertilization, nitrogen deposition, and climate change [14–16]. Additionally, forest disturbance and regeneration processes also play a crucial role [17]. Forest disturbance, which includes physical damage through deforestation and fire-induced mortality, as well as physiological damage through temporary increases in respiration and decreases in photosynthesis, can significantly impact the carbon balance of

forest ecosystems and change forest demography [18–20]. Forest age, commonly estimated as the time since the last major disturbance, is considered a critical parameter that affects the carbon sequestration potential and status of forest ecosystems [21,22]. Recent studies have emphasized the importance of forest age structure in determining carbon sequestration potential at various spatial and temporal scales [17,23,24]. Therefore, forest age can serve as a surrogate for major disturbance information, such as harvest [25], insect-induced mortality [26], and forest fires [27]. However, the effect of forest age has been neglected in many early studies on the estimation of forest carbon balance due to a lack of quantitative knowledge of forest age distribution.

Previously, forest age data were primarily obtained by interpolating statistical information on the age of different forest stands, including natural and planted forests, from national forest inventory (NFI) data [28,29]. The NFI data classify the age of the dominant forest species in each province of China into five classes: young, middle-aged, premature, mature, and overmature. However, the NFI is conducted only every 5 years, making it challenging to obtain explicit information on forest age in both spatial and temporal terms [17]. Wang et al., produced the first national forest age map with a resolution of 1 km using NFI records for 32 provinces in China between 1989 and 1993 [30]. Although the map has facilitated the modeling of forest carbon budgets in China [31,32], it does not adequately reflect grid-based age differences within a province due to the limitations of the NFI data itself. Dai et al., produced a forest age map in China (8 km resolution), which was generated based on the relationship between provincial average stand age from 1994 to 1998 forest inventories and a specific vegetation index (i.e., normalized difference vegetation index, NDVI) [33]. However, as NDVI tends to saturate, this inevitably underestimates high forest ages. Forest age maps have been generated in several studies through the relationship between age and height or spatial downscaling. For instance, Zhang et al., produced a 1 km spatial resolution forest age map by combining forest height and type data with the tree age–height relationship [17]. The authors also developed a top-down forest age downscaling approach to derive a forest stand age map at a 1 km spatial resolution from provincial statistics [23]. Moreover, a machine-learning technique was utilized in another study to estimate the age of global forests based on forest inventory, biomass, and climate data [24]. However, all the forest age data generated by the above studies have neglected the effect of forest disturbance on age. Moreover, due to the low spatial resolution, it is difficult to provide scientific references for the development of forest management measures to increase sink emission reduction. Consequently, it is essential to develop a reliable, spatially explicit, and high-resolution forest age dataset to improve our understanding of forest carbon sequestration capacity.

Extensive archiving of remote-sensing data (e.g., Landsat) provides the ideal option for monitoring natural and anthropogenic landscape changes, such as forest disturbances, at local or regional scales over years and decades [34]. Since the United States Geological Survey (USGS) has made Landsat data freely accessible, there has been rapid development of change-detection algorithms for forest disturbance based on long-term Landsat time-series stacks (LTSS), such as Vegetation Change Tracker (VCT) [35], Breaks For Additive Season and Trend Monitor (BFAST) [36], and Landsat-based Detection of Trends in Disturbance and Recovery (LandTrendr) algorithm [37]. LandTrendr is considered to be one of the best algorithms for detecting forest disturbances due to the effectiveness of the spectral temporal segmentation algorithm in detecting both short-term severe disturbances and long-term slow vegetation change events [37,38]. LTSS provide an ideal choice of data for the LandTrendr algorithm, not only because of the medium spatial resolution and global coverage advantages of LTSS, but also because its decades-long time span supports long-term forest change detection [39]. In addition, the LandTrendr algorithm can directly identify the year of forest disturbance, making it well-suited for estimating the age of disturbed forests. Furthermore, numerous studies have demonstrated a strong correlation between forest age and forest height [17,23]. Therefore, for non-disturbed forests, forest age can be estimated using empirical relationships between age and height [17]. Previous

research has also shown that forest carbon sequestration capacity is closely linked to forest age: younger forests in early stages of succession tend to have higher ecosystem carbon sink potential, while, as overall forest age increases and the proportion of mature and over-mature forests rises, the ecosystem tends to equilibrate and carbon sink capacity gradually decreases [40]. Therefore, forest age data with clear spatial information and high resolution may provide a more accurate estimation of forest carbon strength.

This study proposed a 30 m resolution forest age mapping method that considers forest disturbance. Specifically, the objectives of this study are to (1) estimate the age of disturbed forests using the LandTrendr algorithm based on LTSS data, (2) extract the ages of non-disturbed forests based on the empirical relationship between age and height, and (3) integrate the age information of disturbed and non-disturbed forests to produce a map of forest age at a spatial resolution of 30 m at the provincial scale.

## 2. Methodology

### 2.1. Study Area

The study area is Guangdong Province, located in the southernmost part of mainland China, characterized by a subtropical monsoon climate zone and covering a total area of 179,725 km<sup>2</sup>. It is situated between latitudes 20°09′–25°31′N and longitudes 109°45′–117°20′E (Figure 1a). The province exhibits diverse landform types, including mountains (33.7%), hills (24.9%), terraces (14.2%), and plains (21.7%), with rivers and lakes accounting for only 5.5% of the total land area. The annual average temperature is 21.87 °C, and the average annual precipitation is 1789.3 mm, concentrated primarily from April to September. Moreover, the average annual sunshine hours increase from north to south, ranging from less than 1500 h to more than 2300 h, while the total annual solar radiation ranges from 4200 MJ/m<sup>2</sup> to 5400 MJ/m<sup>2</sup>.

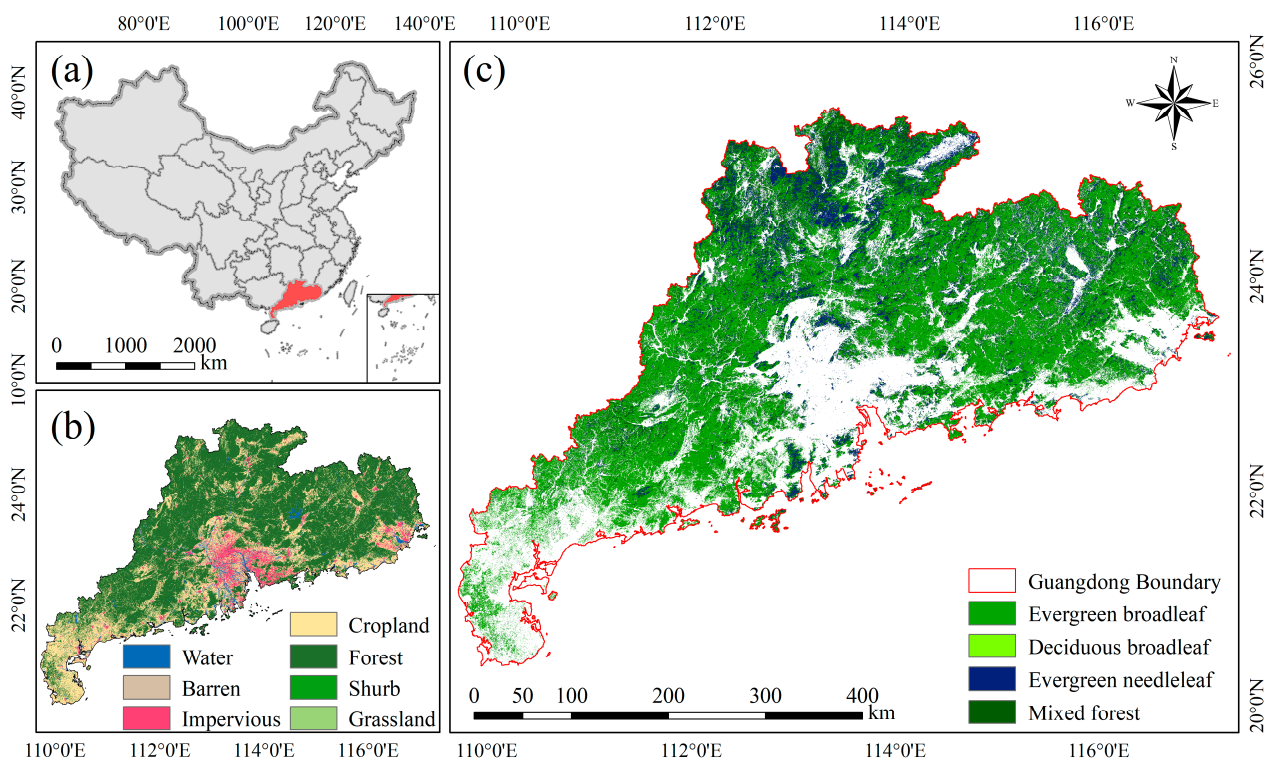


**Figure 1.** Location map of Guangdong Province. (a) location of Guangdong Province in China; (b) land-use classification of Guangdong Province based on the China Land Cover Dataset (CLCD) in 2021 [37]; (c) forest types of Guangdong Province adapted from Li et al. [38].

According to the ninth report of China NFI (2014–2018), the forest area of Guangdong Province is 94,598 km<sup>2</sup>, comprising 4.29% of the national forest area, with a forest coverage

rate of 53.52%. Eucalyptus, fir, and Japanese cedar are the dominant species in Guangdong Province, accounting for 23.90%, 10.32%, and 5.04% of the tree cover area, respectively. Planted forests make up a considerable proportion of the forest area in Guangdong Province, with 61,551 km<sup>2</sup> of planted forests accounting for 65.07%, and 33,047 km<sup>2</sup> of natural forests accounting for 34.93%. As a result of rapid economic development and urbanization in recent years, forest resources in Guangdong Province have been significantly disturbed, resulting in an uneven distribution of forest age with a substantial proportion of young forests. Therefore, it is necessary to accurately map forest age in Guangdong Province to develop appropriate policies to increase carbon sinks and mitigate emissions.

## 2.2. Data Source and Preprocessing

### 2.2.1. Landsat Imagery

We collected all available Tier 1 surface reflectance (SR) data from Landsat 5 Thematic Mapper (TM), Landsat 7 Enhanced Thematic Mapper Plus (ETM+), and Landsat 8 Operational Land Imager (OLI) acquired between May and October from 1986 to 2021 from the Google Earth Engine (GEE) platform. GEE is an online remote-sensing cloud platform that enables efficient computation and analysis of remote-sensing big data [41–43]. All Landsat Level-1 data products are created using the best available processing level for each scene and these data were atmospherically corrected using the Landsat ecosystem disturbance adaptive processing system (LEDAPS) [44] and the Landsat 8 Surface Reflectance Code (LaSRC) algorithm [45] by the USGS. Moreover, cloud, shadow, water, and snow are masked using the C Function of the Mask algorithm [46]. The availability of images for each year and the Landsat sensor is depicted in Figure 2. Considering the good agreement between the TM and ETM+ [47–49], we normalized OLI reflectance using the coefficients proposed by Roy et al. [50]. to mitigate mapping errors arising from differences between OLI and ETM+ sensors. Subsequently, we calculated the annual maximum of the time series of normalized burn ratio (*NBR*) based on Landsat data, which served as input for the LandTrendr algorithm. *NBR* is highly sensitive to forest disturbance and restoration [38,51,52], with higher *NBR* values typically indicating healthy and dense vegetation, and can be calculated using Equation (1).

$$NBR = \frac{NIR - SWIR2}{NIR + SWIR2} \quad (1)$$

where *NIR* and *SWIR2* are the reflectances of Landsat data in near-infrared and short-wave infrared, respectively.

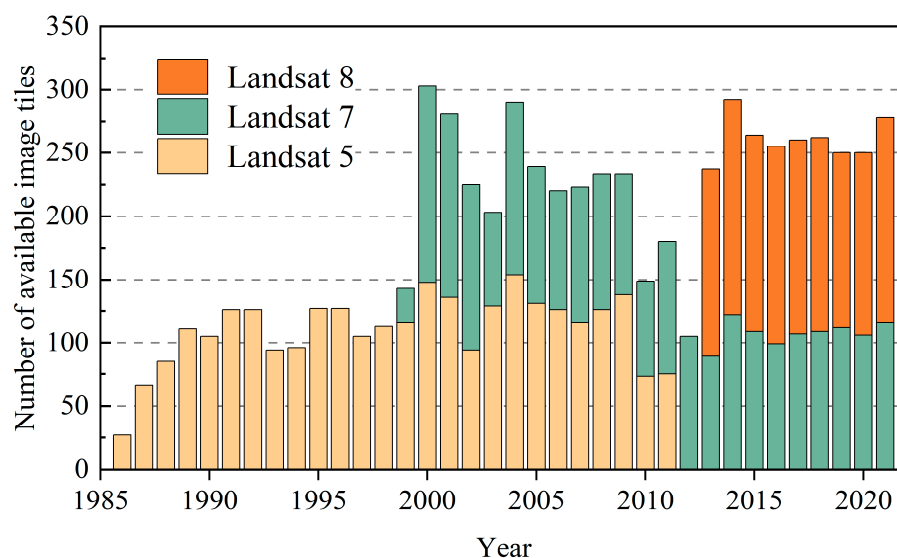


**Figure 2.** Available image tiles from different Landsat sensors in the study area from May to October for the period 1986–2021.

In some areas of the study area, data are missing due to cloud cover and other factors. To generate a complete and continuous time series of NBR data, we defined a null-filling window, which involved using a 3-year sliding window moving backward from 2021. This approach filled the missing NBR data by supplementing the null value of 2021 with the value from the closest year, filling the year with an NBR of 0 with the average of NBR from two adjacent years, and using the value from the next year as a complementary value for years that were null in the previous year. This allowed us to produce NBR time-series data from Landsat images spanning the period from 1986 to 2021.

### 2.2.2. Forest Types and Canopy Height Data

The forest land-use types in Guangdong Province, as determined by the China Land Cover Dataset (CLCD) in 2021 [53], were utilized to delineate the extent of forest cover (Figure 1b). A circa 2010 forest-type map with a spatial resolution of 30 m in China, generated by the State Key Laboratory of Remote-Sensing Science at Beijing Normal University [54], was employed to delineate the distribution of different forest types. Four forest types were classified based on the actual forest distribution in Guangdong Province (Figure 1c), including evergreen broadleaf forest (EBF), deciduous broadleaf forest (DBF), evergreen coniferous forest (ENF), and mixed forest (MF).

The Global Forest Canopy Height Map [55] provides a 30 m resolution map of forest canopy height in the study area (Figure 3a). It will estimate pixel-based forest ages in conjunction with forest-type maps and the appropriate relationship between forest age and forest height.

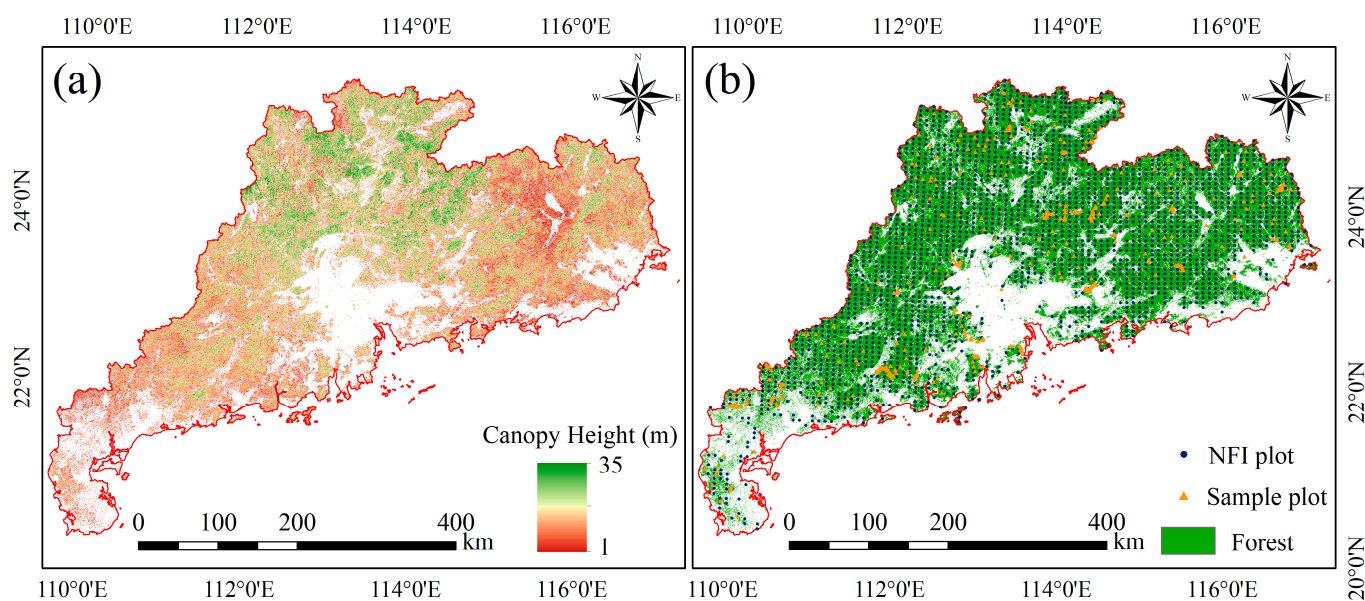


**Figure 3.** (a) Forest canopy height map; (b) Spatial distribution of forest validation sample points.

### 2.2.3. Validation Sampling Data

A total of 2911 sample points were used to validate the estimated forest age and disturbance, primarily consisting of NFI plots, forest management archive data of forestry departments, and visually interpreted plots from high-resolution satellite images obtained from the Google Earth Pro platform and Landsat images (Figure 3b). Statistical information on the age of the different stand origins (natural and planted) for the dominant forest species was provided by the NFI data. The local forestry department's management archive data contains records relating to forest management, such as the time, location, and scale of fires, pest and disease outbreaks, afforestation, and harvest. High-resolution satellite imagery (559 sample points) was used to validate the closest disturbance year detected by the LandTrendr algorithm, which then indicates the accuracy of the age of the disturbed

forest obtained based on the closest disturbance year, while NFI data (2352 sample points) were used to validate non-disturbed forest age.

The high-resolution satellite images included Quick-bird images and 10 m resolution Sentinel-2 panchromatic images (only for the period after 2016), while Landsat images with a resolution of 30 m were collected (263 sample points) to validate forest disturbance years prior to 2000. Sample points were selected using Landsat images as the boundary map, and only sample plots with disturbed areas larger than 30 m × 30 m were included in the validation dataset.

### 2.3. Forest Age Mapping Methods

Forest disturbance significantly impacts forest distribution and directly influences forest age. Combining data from forest disturbance records and forest inventory data can produce accurate forest age data. However, these data are frequently lacking, especially for larger-scale areas. Therefore, according to the criteria of whether there was a disturbance during the study period, we classified the forest into disturbed and non-disturbed areas and mapped their respective age (see Figure 4). Specifically, disturbed forest age was determined using the LandTrendr algorithm, while non-disturbed forest age was estimated using the empirical relationship between age and height.

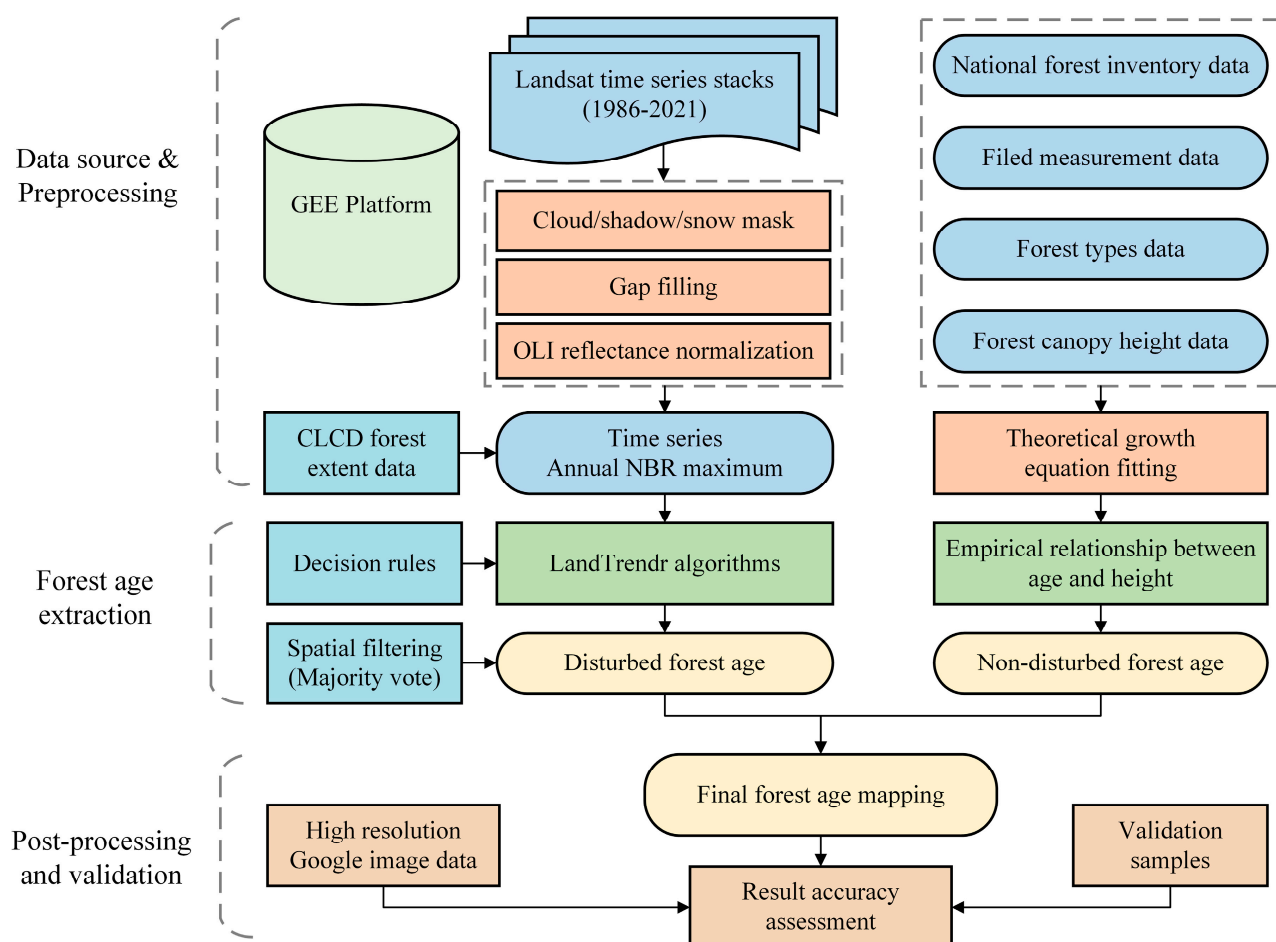


**Figure 4.** Workflow for forest age mapping.

#### 2.3.1. Disturbed Forest Age Mapping

Forest disturbances, such as harvest, insect-induced mortality, and forest fires, can be estimated using the LandTrendr algorithm implemented on GEE to determine the age of the disturbed forest based on the year of the most recent disturbance [56], i.e., the difference between 2021 and the year of the closest disturbance year is the age of the disturbed forest.

The algorithm first removes ephemeral spikes (noise) due to clouds, shadows, etc., then identifies the optimal vertices and removes the redundant vertices based on the regression line, subsequently forming the best continuous spectral indicator trajectory in the complete time series based on a variety of fitting rules, and finally simplifies the model and selects the best fitting model. The parameter settings for LandTrendr in this study were consistent with previous studies [57,58].

The LandTrendr algorithm requires NBR time-series data from 1986 to 2021 as input, and generates four bands as output, namely the year of observation, the original observation, the fitted observation, and a Boolean value to indicate whether the observation is identified as a vertex. First, the LTSS is pre-processed to generate long time series of NBR data, including clouds, shadow masks, null padding, sensor reflectance normalization, etc. The main objective of this study was to identify the most recent year of disturbance for each pixel, as multiple segments were often detected by LandTrendr for most pixels. To address the issue of detections, we established two decision rules: (1) the segment duration must be greater than 1 year, and (2) the delta of the fitted observation value in the segment must be greater than 0.2. Subsequently, the start vertex observation year was selected as the most recent year of disturbance. For pixels that failed to satisfy the decision rules, we identified the segment with the largest increase in NBR and regarded the start vertex as the most recent year of disturbance. The forest areas that meet the above rules are classified as disturbed forests, and pixels that lacked an increasing segment were categorized as non-disturbed forest pixels. Moreover, a  $3 \times 3$  spatial filtering window with a “majority vote” rule [59] was implemented on the output to reduce the “salt and pepper” effect.

### 2.3.2. Non-Disturbed Forest Age Mapping

For non-disturbed forest pixels, age will be extracted based on the empirical relationship between forest canopy height and age. The empirical relationship between age and height for the different forest types in the study area was obtained from Zhang et al. [17], using a theoretical growth equation fitting (Table 1), which was fitted based on theoretical growth equations using data from 3543 publicly available sampling plots in China. These plots have a wide range of forest types and plot conditions that support the establishment of age and height relationships.

**Table 1.** Relationships between age and height for different forest types in the study area (reference Zhang et al. [17]). Note: A and H represent age and height, respectively.

Forest Types	Forest Age Formula	Application Conditions
EBF	$A = 778.8843 - 121.9512 \ln(640.7587 - 1.0782 H^{1.7549})$	$8.5703 < H < 38.0815$
DBF	$A = 8.2131 / (5.7062 - 1.6733 \ln(H))^{0.899}$	$0 < H < 30.2697$
ENF	$A = 28.1507 - 12.4533 \ln(67.4215 H^{-1.2521} - 1)$	$4.3864 < H < 28.8792$
MF	$A = 25.0465 - 4.89 \ln(65.012 H^{-1.3619} - 1)$ $A = 21.4927 / (4.4971 - 1.3569 \ln(H))^{1.5891}$	$0.4966 < H < 21.4399$ $0 < H < 27.5016$

Based on the above LandTrendr algorithm determined as non-disturbed forest pixels, we classify them into four forest types for separate age extraction. Based on the canopy height data corresponding to different forest types, the empirical relationship between height and age in Table 1 was applied to obtain the age of the non-disturbed forest.

## 3. Results

### 3.1. Disturbance Forest Age and Validation

The closest detected disturbance year of the forest in Guangdong Province, using the LandTrendr algorithm, is presented in Figure 5. The accuracy of the acquired closest disturbance year was verified using high-resolution Google images combined with the forest management archive data of local forestry departments. The LandTrendr algorithm demonstrates high accuracy in detecting disturbance years, with producer and user accura-

cies of approximately 94% and 95%, respectively, and the kappa coefficient was 0.89, based on 1036 validation points from high-resolution Google images (Figure 6). Despite some mixed pixels in the Landsat image compared to the high-resolution image, the disturbed areas can still be accurately discerned based on the Landsat image. However, there may be some mixed-pixel mismatches in the edge regions of the disturbed forest. The fitted NBR values at selected sample points confirm that the LandTrendr algorithm successfully detected the closest disturbance years of the forest in Guangdong Province in 2015, 2017, and 2011, indicating the feasibility of obtaining the age trajectory of the disturbed forest using the LandTrendr algorithm.

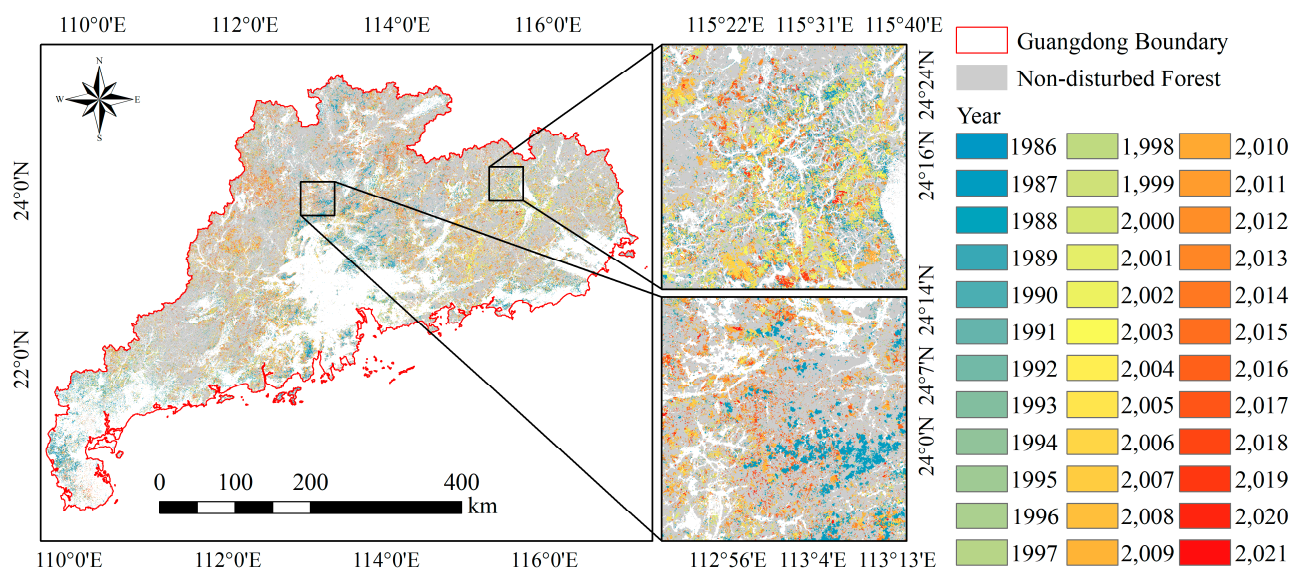


**Figure 5.** Year of closest forest disturbance.

As a result, we successfully obtained the disturbed forest age in Guangdong Province from 1986 to 2021 (Figure 7). Figure 7 illustrates that the forest disturbance area is mainly located in the central and northwestern parts of Guangdong Province, where the land-use types are cropland and artificial surface (impervious) (Figure 1b). Statistical analysis of the age of disturbed forests reveals that the highest percentage of area is occupied by forests aged 21 to 31 years, followed by forests aged 11 to 20 years, and the lowest by forests aged 6 to 10 years (Table 2). This observation also reflects that the most intense level of forest disturbance in Guangdong Province occurred between 1991 and 2000. Additionally, the proportion of forest area disturbed within 1 to 5 years is 24.45%, indicating a relatively high degree of forest disturbance in Guangdong Province in the past 5 years.

**Table 2.** Statistics of the age of disturbed forests.

Age of Disturbed Forest (Year)	Area (km <sup>2</sup> )	Proportion of Disturbed Forest Area (%)
1–5	8440.91	24.45
6–10	2333.12	6.76
11–20	7861.63	22.77
21–30	12,669.52	36.69
31–40	3222.60	9.33
Total	34,527.78	100

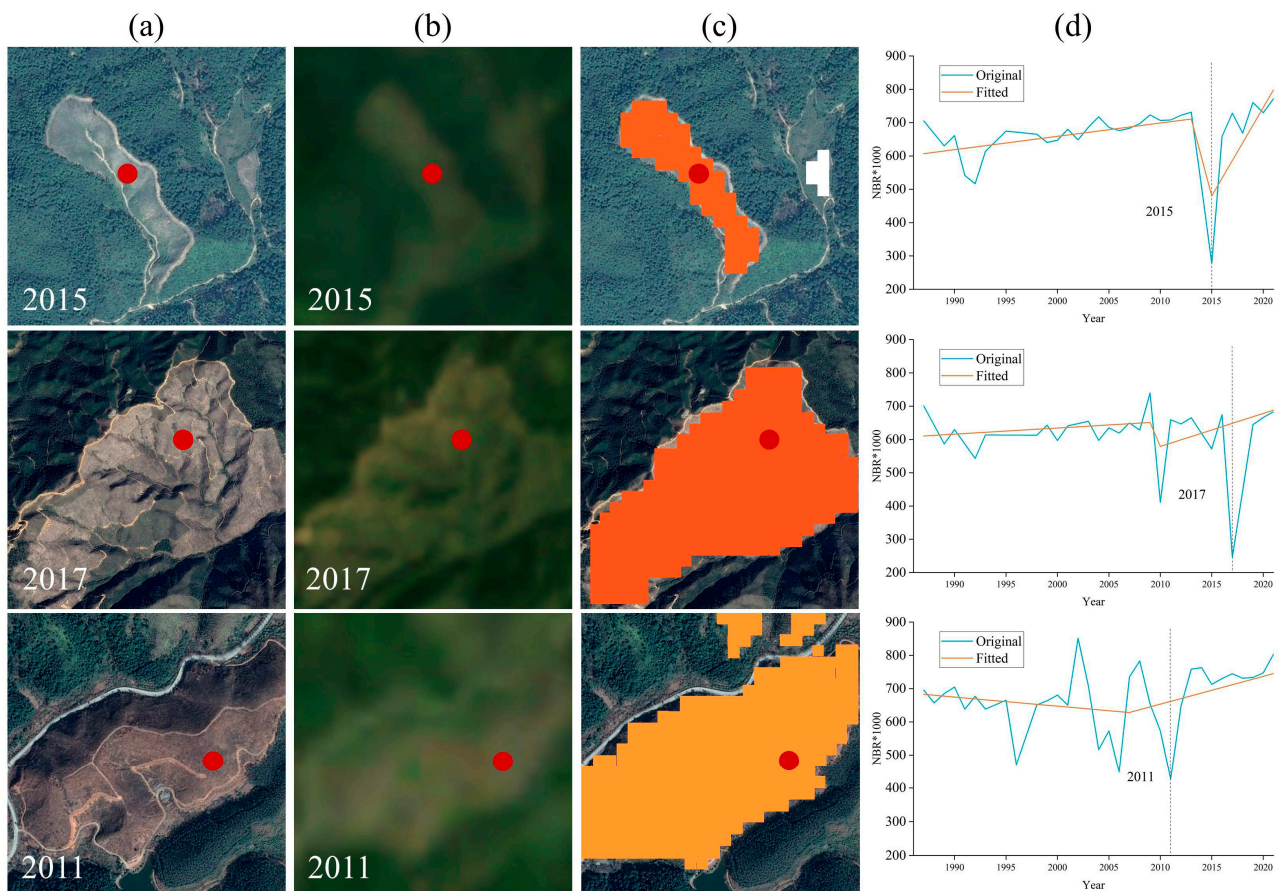


**Figure 6.** Disturbed forest year validation based on high-resolution images in the Google Earth Pro platform (<https://earth.google.com/web/>, accessed on 7 April 2023). (a) Google high-resolution images; (b) Landsat images; (c) the year of disturbance detected by the LandTrendr algorithm; (d) Fitting disturbance trajectories for NBR. Note: the red dots are the sampling plots, which are also the points for fitting the disturbance trajectories.

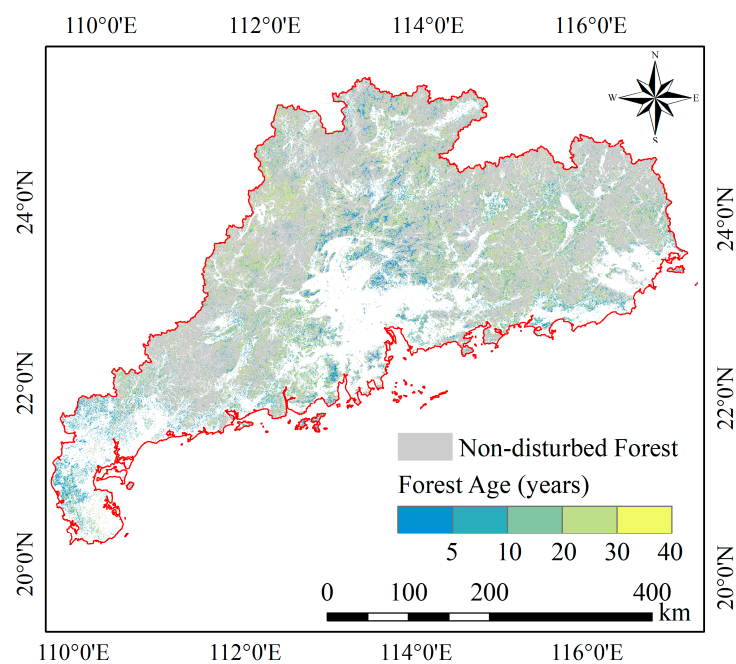


**Figure 7.** Disturbed forest age mapping.

### 3.2. Non-Disturbed Forest Age and Validation

Based on the forest canopy height data provided by the Global Forest Canopy Height Map for Guangdong Province, we applied the empirical relationship between age and height for different forest types to obtain the age of non-disturbed forests, as depicted in Figure 8. Benefiting from the forest age data from the 9th NFI report (2352 sample points), we validated the estimated age of non-disturbed forests. The correlation analysis between age and height estimates and NFI results revealed that the coefficient of determination  $R^2$  value of 0.8875 and the root mean squared error (RMSE) value of 5.776 between age obtained using empirical age–height relationships and the NFI-based survey results, indicating a higher degree of consistency between the two approaches (Figure 9). Scatter points smaller than 50 years showed a higher concentration on both sides of the trend line, whereas scatters larger than 50 years appeared more dispersed. Overall, the results of this accuracy assessment suggest that forest ages can be estimated with a relatively higher accuracy using the empirical relationship between age and height for different forest types, although the accuracy may decrease for older forests (greater than 50 years).

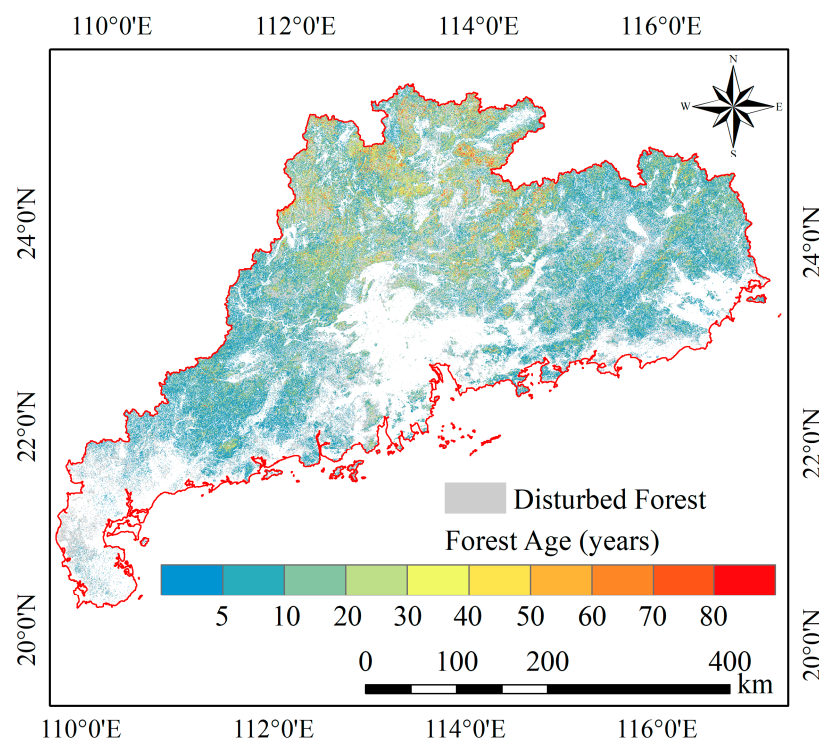


**Figure 8.** Non-disturbed forest age mapping.

Older forests in non-disturbed areas are primarily located in the northern part of Guangdong Province, while younger forests are mainly distributed in the eastern and western parts of the province (Figure 8). Statistical data on the age of non-disturbed forests reveal that 52.33% of the forests in Guangdong Province are less than 10 years old, 45.11% are between 10 and 50 years old, and only 2.56% are over 50 years old (Table 3).

### 3.3. Final Forest Age Mapping

A forest age map of Guangdong Province (2021 year) was generated using age data on disturbed and non-disturbed forests (Figure 10). The average age of forests in Guangdong Province is 15.1 years, with forests less than 40 years old comprising 63% of the total forest area. Guangdong Province has been a key area for national afforestation efforts since the late 1970s, resulting in a relatively high proportion of young forests, particularly in the eastern and western parts of the province. The young age of the forests in Guangdong Province is attributed to the intense human disturbance and recent afforestation policies.

Forests older than 50 years account for 19% of the total forest area and are primarily located in the higher altitude northern mountainous areas (Figure 1b), such as the mountains surrounding Qingyuan City and Shaoguan City (e.g., Shikengkong, Paradise Ridge, etc.).

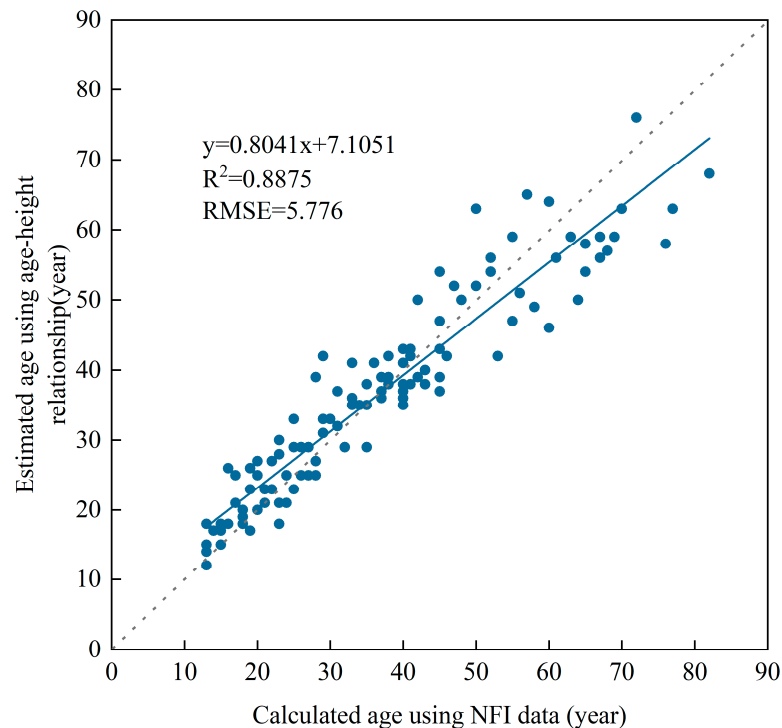


**Figure 9.** Validation of the age of non-disturbed forests based on NFI data. Note: RMSE, root mean squared error.

**Table 3.** Statistics of the age of non-disturbed forests.

Age of Non-Disturbed Forest (Year)	Area (km <sup>2</sup> )	Proportion of Non-Disturbed Forest Area (%)
1–5	20,431.55	25.71
6–10	21,154.50	26.62
11–20	19,504.53	24.55
21–30	11,215.77	14.12
31–40	3725.30	4.69
41–50	1392.82	1.75
51–60	663.29	0.83
61–70	555.37	0.70
71–80	13.51	0.02
>80	802.76	1.01
Total	79,459.40	100

Figure 11 illustrates the histogram depicting forest age distribution among different forest types. Deciduous broadleaf forests exhibit the youngest average age at 8.57 years, followed by evergreen broadleaf forests at 12.64 years, and evergreen coniferous forests at 16.89 years. Mixed forests, on the other hand, exhibit the highest average age at 22.07 years. Notably, forests that are less than 20 years old account for over 69% of the total forest area, primarily due to afforestation activities. The rapid increase in planted forests in Guangdong Province over the past few decades likely explains the relatively younger age of forests in this region. Although mixed forests include some older non-disturbed forests, the other three forest types exhibit a small percentage of forests with an age greater than 50 years. This may be due to inaccurate age extraction resulting from lower forest-type classification accuracy, as well as local variations in forest species distribution and forest-type selection

for afforestation activities. Thus, the higher average age in mixed forests can be attributed to the inclusion of older natural forests in this forest type.

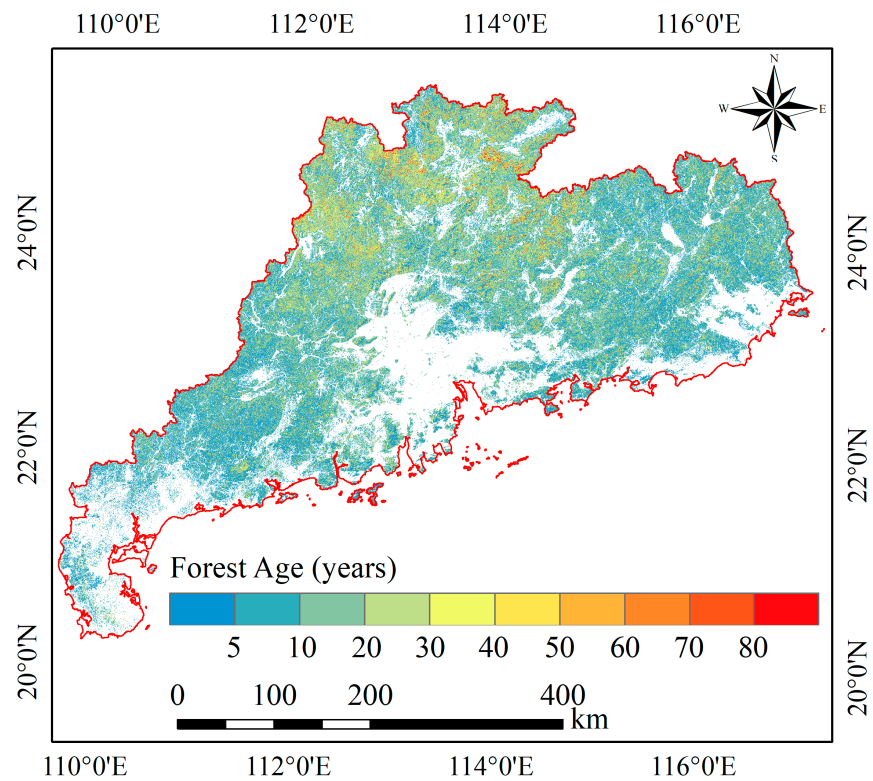


Figure 10. Final forest age map in Guangdong Province (2021 year).

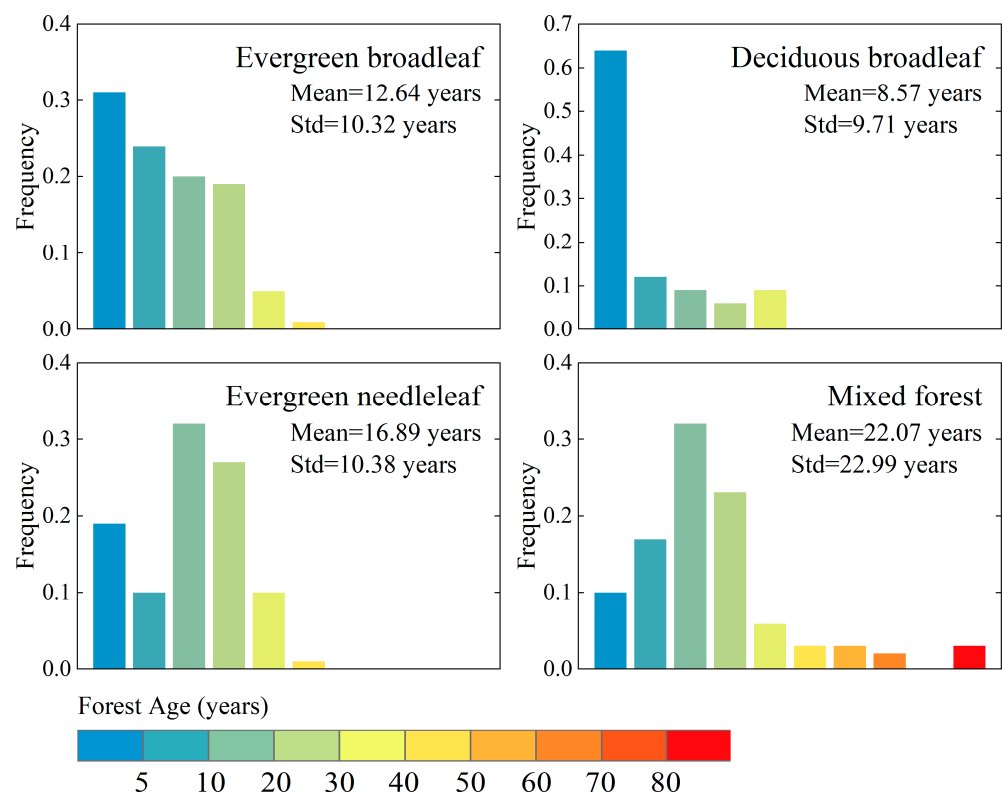


Figure 11. Histograms of forest age of each forest type.

## 4. Discussion

### 4.1. Methodology for Forest Age Estimation

The total area of forests that have experienced disturbance in Guangdong Province since 1986 is estimated to be approximately 34,527.78 km<sup>2</sup>, which accounts for 30.29% of the total forest area in Guangdong Province, based on the forest-type area data from the 2021 CLCD [53] (Figure 1c). Li et al., reported that deforestation in southern China during the period 1980–1990 was approximately 13.5% of the forest area, consistent with data from the NFI [60]. Xian et al. [61] showed that forest change losses in Guangdong Province between 1980 and 2015 were mainly influenced by economically oriented factors, although deforestation driven by economic factors was limited by forest management policies. In addition, the “Guidance on Strengthening the Management of Collective Forest Resources and Prohibiting Indiscriminate Logging in the South” was promulgated in 1987 to curb the uncontrolled logging resulting from the “three determinations” policy; however, forest disturbance in Guangdong Province has remained high over recent decades [38]. Since mature and overmature forests are almost completely logged, consequently, the remaining disturbed forests also tend to be younger.

Statistical information on the age of non-disturbed forests indicates extensive afforestation efforts undertaken in Guangdong Province over the past decade. The forest area in Guangdong Province has continuously increased due to the implementation of two major afforestation projects in China, namely the Fast-growing and High-yield Plantation in Key Areas project [62], which protects natural forests from deforestation while meeting the timber demand of the Chinese market, and the Grain to Green Program [63,64], which aims to convert cultivated land to forest land to increase forest area and mitigate soil erosion. According to the Guangdong Statistical Yearbooks, the forest area in Guangdong Province has increased from 59,840 km<sup>2</sup> in 1980 to 105,241 km<sup>2</sup> in 2020, with an average annual growth rate of 1.90% [65]. These policies have contributed to the substantial area increase in non-disturbed forests in Guangdong Province that are less than 20 years old, accounting for 76.88% of the total forest area from 2003 to 2019.

The forest ages obtained in this study are comparable to those obtained in previous studies [23,33]. However, our approach, which considers the effects of forest disturbance on age and utilizes long-time-series remote-sensing imagery, not only reflects more detailed spatial variation in forest age but also achieves a higher resolution. Forest age serves as a proxy for time since disturbance implicitly reflects the legacy of past disturbances [66]. Forest inventory data, combined with historical forest disturbance information, can be used to generate accurate forest age maps [66]. However, spatially distributed forest inventory and disturbance data are not universally available. Therefore, the method proposed in this study, which extracts ages from remote-sensing data based on LTSS and forest height while considering forest disturbance, has the potential for widespread use in various regions worldwide. With the continued development and application of satellite-based laser data, it may be possible to obtain annual remotely sensed forest height data in the future, enabling the method to achieve annual estimates of forest age.

### 4.2. Uncertainties in Forest Age Map

Global coverage and decades-long time series of Landsat data offer optimal opportunities for the monitoring of natural and anthropogenic landscape changes at various spatial and temporal scales [34,67]. However, limitations such as cloud cover, technical constraints, and data failures have led to gaps in the availability of continuous Landsat data in certain regions [46,68]. Despite these limitations, we implemented a sliding window approach to fill in the missing Landsat data. Nevertheless, this approach may introduce uncertainties in the detection of forest disturbance years by the LandTrendr algorithm, which in turn could result in errors in estimating the age of disturbed forests. A more accurate method for filling in missing values would help minimize the uncertainty arising from data gaps.

The forest-type data with a resolution of 30 m utilized in this study is the 2010 forest-type map developed by Li et al. [54] (Figure 1c). The accuracy of forest-type distribution

directly impacts the accuracy of age extraction for different forest types, as age and height estimation rely on different empirical formulas for each forest type (Table 1). Moreover, the age and height empirical relationships are derived from growth equations, which inherently contain uncertainties. Furthermore, the forest height map used in this study is considered one of the most comprehensive descriptions of global forest vertical structure available, based on the work of Potapov et al. [55]. We compared the forest canopy height data in this study with other forest canopy height data, such as the global 1 km canopy height map [69]. The results show that the two products show good consistency in Guangdong Province in general, with the high and low-value areas being more similarly distributed. The global 1 km canopy height map has a higher maximum value (40 m), which may be due to the different sources of the two types of forest canopy height data and the different resolutions of the two data products [55,69]. However, it should be noted that the accuracy of the forest height map may be affected by uncertainties in Global Ecosystem Dynamics Investigation LiDAR calibration, particularly in geolocation precision and land surface height estimation, which could contribute to map errors [55]. Additionally, the forest height model employed in this study saturates above 30 m and may not accurately represent the height of the tallest trees. Moreover, a few forest height values exceeded the boundary conditions for the age–height relationship, which could have resulted in the underestimation of the age of older forests [17]. Therefore, future research should consider using spatially explicit forest-type and height data, as well as higher-precision empirical relationships between age and height, to enhance the accuracy of forest age estimates.

In this study, we used high-resolution Google images combined with the forest management archive data of forestry departments and NFI data to validate the ages of disturbed and non-disturbed forests, respectively. However, the age of the early disturbed forests could not be confirmed due to the unavailability of high-resolution Google images prior to 2000. Fortunately, we successfully validated the applicability of the LandTrendr algorithm for detecting the age of disturbed forests using high-resolution Google images (Figure 6). Notably, in NFI data, the forest age is calculated as an area-weighted average of the median values of different age classes estimated for all forest types, which is a widely accepted method for estimating average forest age based on NFI data. However, this approach may introduce some uncertainties [33]. Currently, provincial NFI data are used to validate forest ages at a resolution of 30 m pixels, which may result in a scale mismatch between field observations and model estimates, potentially impacting the validation results [17]. Nevertheless, it is important to highlight that NFI data currently represents the most reliable dataset for validating pixel-based estimates of forest age, as it provides comprehensive information on the spatial distribution of forest age [17]. Despite all the above limitations, the forest age mapping method proposed in this study offers a novel approach to mapping forest age by considering forest disturbance with high spatial resolution, therefore contributing to the sustainable management of forest resources and a better understanding of carbon budget studies in forest ecosystems.

## 5. Conclusions

As a major surrogate for forest disturbance, forest age plays a crucial role in determining the intensity of terrestrial carbon sources or sinks. In this study, we utilized the LandTrendr algorithm, a forest disturbance algorithm, to extract the age of disturbed forests based on LTSS data from 1986 to 2021. Additionally, we estimated the age of non-disturbed forests using forest height data and an empirical relationship between age and height. This allowed us to generate a high-resolution (30 m) map of forest age for Guangdong Province. Validation results using high-resolution Google images, the forest management archive data of forestry departments, and NFI data demonstrated that our proposed method is highly accurate in capturing forest disturbance and mapping forest age at a 30 m resolution using remote-sensing data. Furthermore, our findings revealed that most forests in Guangdong Province are relatively young, with forests less than 20 years old accounting for 69.94% of the total forest area, which not only accounts for forest disturbance but also for extensive

afforestation activities. The accuracy of forest age mapping is highly dependent on the availability and reliability of multiple remote-sensing data, including Landsat imagery, forest-type information, and forest height data, as well as the relationship between age and height. Minimizing sources of uncertainty associated with these factors would enhance the accuracy of estimated forest ages. Overall, the results of this study contribute to a better understanding of the carbon budget of forest ecosystems and the sustainable management of forest resources.

**Author Contributions:** Conceptualization, L.T. and M.L.; visualization, L.L., Y.T. and X.W.; formal analysis, Y.T. and X.W.; writing—original draft preparation and editing, L.T., Y.T. and M.L.; funding acquisition, L.T. and M.L. All authors have read and agreed to the published version of the manuscript.

**Funding:** This research was funded by the Postgraduate Research & Practice Innovation Program of Jiangsu Province, and the National Natural Science Foundation of China (31770679).

**Data Availability Statement:** Not applicable.

**Acknowledgments:** The authors would like to thank the Finer Resolution Observation and Monitoring–Global Land Cover (<http://data.ess.tsinghua.edu.cn/>, accessed on 10 February 2023), and the Global Forest Canopy Height Map (<https://glad.umd.edu/dataset/gedi/>; accessed on 10 February 2023) for providing data support. The authors thank the Google Earth Pro platform (<https://earth.google.com/web/>, accessed on 7 April 2023) for the high-resolution images. In addition, we are thankful for all the helpful comments provided by the reviewers.

**Conflicts of Interest:** The authors declare no conflict of interest.

## References

1. Tian, L.; Fu, W. Bi-Temporal Analysis of Spatial Changes of Boreal Forest Cover and Species in Siberia for the Years 1985 and 2015. *Remote Sens.* **2020**, *12*, 4116. [[CrossRef](#)]
2. Bair-On, Y.M.; Phillips, R.; Milo, R. The biomass distribution on Earth. *Proc. Natl. Acad. Sci. USA* **2018**, *115*, 6506–6511. [[CrossRef](#)] [[PubMed](#)]
3. Lei, H.Q.; Sun, G.Q.; Zheng, D.L. Carbon storage of forest ecosystem in Wenzhou City, Zhejiang Province, China. *J. Nanjing For. Univ.* **2022**, *46*, 20–26. [[CrossRef](#)]
4. Houghton, R.A.; Hall, F.; Goetz, S.J. Importance of biomass in the global carbon cycle. *J. Geophys. Res. Biogeosci.* **2009**, *114*, G00E03. [[CrossRef](#)]
5. Pan, Y.D.; Birdsey, R.A.; Fang, J.Y.; Houghton, R.; Kauppi, P.E.; Kurz, W.A.; Phillips, O.L.; Shvidenko, A.; Lewis, S.L.; Canadell, J.G.; et al. A Large and Persistent Carbon Sink in the World's Forests. *Science* **2011**, *333*, 988–993. [[CrossRef](#)]
6. Molotoks, A.; Stehfest, E.; Doelman, J.; Albanito, F.; Fitton, N.; Dawson, T.P.; Smith, P. Global projections of future cropland expansion to 2050 and direct impacts on biodiversity and carbon storage. *Glob. Chang. Biol.* **2018**, *24*, 5895–5908. [[CrossRef](#)]
7. Payne, N.J.; Cameron, D.A.; Leblanc, J.D.; Morrison, I.K. Carbon storage and net primary productivity in Canadian boreal mixedwood stands. *J. For. Res.* **2019**, *30*, 1667–1678. [[CrossRef](#)]
8. Xiao, J.F.; Chevallier, F.; Gomez, C.; Guanter, L.; Hicke, J.A.; Huete, A.R.; Ichii, K.; Ni, W.J.; Pang, Y.; Rahman, A.F.; et al. Remote sensing of the terrestrial carbon cycle: A review of advances over 50 years. *Remote Sens. Environ.* **2019**, *233*, 111383. [[CrossRef](#)]
9. Tian, L.; Tao, Y.; Fu, W.X.; Li, T.; Ren, F.; Li, M.Y. Dynamic Simulation of Land Use/Cover Change and Assessment of Forest Ecosystem Carbon Storage under Climate Change Scenarios in Guangdong Province, China. *Remote Sens.* **2022**, *14*, 2330. [[CrossRef](#)]
10. Wang, D.W.; Shen, W.X. The carbon storage calculation and carbon sequestration potential analysis of the main artificial arboreal forest in China. *J. Nanjing For. Univ.* **2022**, *46*, 11–19. [[CrossRef](#)]
11. Tao, Y.; Tian, L.; Wang, C.; Dai, W. Dynamic simulation of land use and land cover and its effect on carbon storage in the Nanjing metropolitan circle under different development scenarios. *Front. Ecol. Evol.* **2023**, *11*, 1102015. [[CrossRef](#)]
12. Tian, L.; Fu, W.X.; Tao, Y.; Li, M.Y.; Wang, L. Dynamics of the alpine timberline and its response to climate change in the Hengduan mountains over the period 1985–2015. *Ecol. Indic.* **2022**, *135*, 108589. [[CrossRef](#)]
13. Ju, Y.L.; Ji, Y.J.; Huang, J.M.; Zhang, W.F. Inversion of forest aboveground biomass using combination of LiDAR and multispectral data. *J. Nanjing For. Univ.* **2022**, *46*, 58–68. [[CrossRef](#)]
14. Zhu, Z.C.; Piao, S.L.; Myneni, R.B.; Huang, M.T.; Zeng, Z.Z.; Canadell, J.G.; Ciais, P.; Sitch, S.; Friedlingstein, P.; Arneeth, A.; et al. Greening of the Earth and its drivers. *Nat. Clim. Chang.* **2016**, *6*, 791–795. [[CrossRef](#)]
15. Winkler, A.J.; Myneni, R.B.; Hannart, A.; Sitch, S.; Haverd, V.; Lombardozi, D.; Arora, V.K.; Pongratz, J.; Nabel, J.; Goll, D.S.; et al. Slowdown of the greening trend in natural vegetation with further rise in atmospheric CO<sub>2</sub>. *Biogeosciences* **2021**, *18*, 4985–5010. [[CrossRef](#)]

16. Fu, W.X.; Tian, L.; Tao, Y.; Li, M.Y.; Guo, H.D. Spatiotemporal changes in the boreal forest in Siberia over the period 1985–2015 against the background of climate change. *Earth Syst. Dyn.* **2023**, *14*, 223–239. [[CrossRef](#)]
17. Zhang, C.H.; Ju, W.M.; Chen, J.M.; Li, D.Q.; Wang, X.Q.; Fan, W.Y.; Li, M.S.; Zan, M. Mapping forest stand age in China using remotely sensed forest height and observation data. *J. Geophys. Res. Biogeosci.* **2014**, *119*, 1163–1179. [[CrossRef](#)]
18. Liu, S.G.; Bond-Lamberty, B.; Hicke, J.A.; Vargas, R.; Zhao, S.Q.; Chen, J.; Edburg, S.L.; Hu, Y.M.; Liu, J.X.; McGuire, A.D.; et al. Simulating the impacts of disturbances on forest carbon cycling in North America: Processes, data, models, and challenges. *J. Geophys. Res. Biogeosci.* **2011**, *116*, G00K08. [[CrossRef](#)]
19. Williams, C.A.; Collatz, G.J.; Masek, J.; Goward, S.N. Carbon consequences of forest disturbance and recovery across the conterminous United States. *Glob. Biogeochem. Cycl.* **2012**, *26*, GB1005. [[CrossRef](#)]
20. Woodbury, P.B.; Smith, J.E.; Heath, L.S. Carbon sequestration in the US forest sector from 1990 to 2010. *For. Ecol. Manag.* **2007**, *241*, 14–27. [[CrossRef](#)]
21. Goulden, M.L.; McMillan, A.M.S.; Winston, G.C.; Rocha, A.V.; Manies, K.L.; Harden, J.W.; Bond-Lamberty, B.P. Patterns of NPP, GPP, respiration, and NEP during boreal forest succession. *Glob. Chang. Biol.* **2011**, *17*, 855–871. [[CrossRef](#)]
22. Poorter, L.; Bongers, F.; Aide, T.M.; Almeyda Zambrano, A.M.; Balvanera, P.; Becknell, J.M.; Boukili, V.; Brancalion, P.H.S.; Broadbent, E.N.; Chazdon, R.L.; et al. Biomass resilience of Neotropical secondary forests. *Nature* **2016**, *530*, 211–214. [[CrossRef](#)]
23. Zhang, Y.; Yao, Y.T.; Wang, X.H.; Liu, Y.W.; Piao, S.L. Mapping spatial distribution of forest age in China. *Earth Space Sci.* **2017**, *4*, 108–116. [[CrossRef](#)]
24. Besnard, S.; Koirala, S.; Santoro, M.; Weber, U.; Nelson, J.; Gutter, J.; Herault, B.; Kassi, J.; N’Guessan, A.; Neigh, C.; et al. Mapping global forest age from forest inventories, biomass and climate data. *Earth Syst. Sci. Data* **2021**, *13*, 4881–4896. [[CrossRef](#)]
25. Zhang, F.M.; Chen, J.M.; Pan, Y.D.; Birdsey, R.A.; Shen, S.H.; Ju, W.M.; He, L.M. Attributing carbon changes in conterminous U.S. forests to disturbance and non-disturbance factors from 1901 to 2010 (vol. 117, G02021, 2012). *J. Geophys. Res. Biogeosci.* **2013**, *118*, 1345–1346. [[CrossRef](#)]
26. Fei, S.L.; Morin, R.S.; Oswalt, C.M.; Liebhold, A.M. Biomass losses resulting from insect and disease invasions in US forests. *Proc. Natl. Acad. Sci. USA* **2019**, *116*, 17371–17376. [[CrossRef](#)] [[PubMed](#)]
27. Taylor, A.H. Fire disturbance and forest structure in an old-growth *Pinus ponderosa* forest, southern Cascades, USA. *J. Veg. Sci.* **2010**, *21*, 561–572. [[CrossRef](#)]
28. Qian, C.H.; Zhao, Y.C.; Li, M.Y.; Li, T. Dynamic analyses of forest ecological functions based on fixed plot data of continuous forest resources inventories from 1979 to 2012 in Guangzhou. *J. Nanjing For. Univ.* **2022**, *46*, 205–212. [[CrossRef](#)]
29. Xu, E.Y.; Nie, Y.; Rui, X.D. Analysis on the forest land use efficiency changes based on forest resource inventory data. *J. Nanjing For. Univ.* **2022**, *46*, 213–220. [[CrossRef](#)]
30. Wang, S.; Chen, J.M.; Ju, W.M.; Feng, X.; Chen, M.; Chen, P.; Yu, G. Carbon sinks and sources in China’s forests during 1901–2001. *J. Environ. Manag.* **2007**, *85*, 524–537. [[CrossRef](#)]
31. Ju, W.M.; Chen, J.M.; Harvey, D.; Wang, S. Future carbon balance of China’s forests under climate change and increasing CO<sub>2</sub>. *J. Environ. Manag.* **2007**, *85*, 538–562. [[CrossRef](#)]
32. Wang, S.Q.; Zhou, L.; Chen, J.M.; Ju, W.M.; Feng, X.F.; Wu, W.X. Relationships between net primary productivity and stand age for several forest types and their influence on China’s carbon balance. *J. Environ. Manag.* **2011**, *92*, 1651–1662. [[CrossRef](#)] [[PubMed](#)]
33. Dai, M.; Zhou, T.; Yang, L.L.; Jia, G.S. Spatial pattern of forest ages in China retrieved from national-level inventory and remote sensing imageries. *Geogr. Res.* **2011**, *30*, 172–184.
34. Rendeniaks, Z.; Nita, M.D.; Nikodemus, O.; Radeloff, V.C. Half a century of forest cover change along the Latvian-Russian border captured by object-based image analysis of Corona and Landsat TM/OLI data. *Remote Sens. Environ.* **2020**, *249*, 112010. [[CrossRef](#)]
35. Huang, C.Q.; Coward, S.N.; Masek, J.G.; Thomas, N.; Zhu, Z.L.; Vogelmann, J.E. An automated approach for reconstructing recent forest disturbance history using dense Landsat time series stacks. *Remote Sens. Environ.* **2010**, *114*, 183–198. [[CrossRef](#)]
36. DeVries, B.; Verbesselt, J.; Kooistra, L.; Herold, M. Robust monitoring of small-scale forest disturbances in a tropical montane forest using Landsat time series. *Remote Sens. Environ.* **2015**, *161*, 107–121. [[CrossRef](#)]
37. Kennedy, R.E.; Yang, Z.G.; Cohen, W.B. Detecting trends in forest disturbance and recovery using yearly Landsat time series: 1. LandTrendr—Temporal segmentation algorithms. *Remote Sens. Environ.* **2010**, *114*, 2897–2910. [[CrossRef](#)]
38. Shen, J.N.; Chen, G.S.; Hua, J.W.; Huang, S.; Ma, J.M. Contrasting Forest Loss and Gain Patterns in Subtropical China Detected Using an Integrated LandTrendr and Machine-Learning Method. *Remote Sens.* **2022**, *14*, 3238. [[CrossRef](#)]
39. Wulder, M.A.; Roy, D.P.; Radeloff, V.C.; Loveland, T.R.; Anderson, M.C.; Johnson, D.M.; Healey, S.; Zhu, Z.; Scambos, T.A.; Pahlevan, N.; et al. Fifty years of Landsat science and impacts. *Remote Sens. Environ.* **2022**, *280*, 113195. [[CrossRef](#)]
40. Piao, S.L.; Yue, C.; Ding, J.Z.; Guo, Z.T. The Role of Terrestrial Ecosystem Carbon Sinks in the “Carbon Neutrality” Goal. *Scientia Sinica* **2022**, *52*, 1419–1442.
41. Ermida, S.L.; Soares, P.; Mantas, V.; Gottsche, F.M.; Trigo, I.E. Google Earth Engine Open-Source Code for Land Surface Temperature Estimation from the Landsat Series. *Remote Sens.* **2020**, *12*, 1471. [[CrossRef](#)]
42. Gorelick, N.; Hancher, M.; Dixon, M.; Ilyushchenko, S.; Thau, D.; Moore, R. Google Earth Engine: Planetary-scale geospatial analysis for everyone. *Remote Sens. Environ.* **2017**, *202*, 18–27. [[CrossRef](#)]
43. Kumar, L.; Mutanga, O. Google Earth Engine Applications Since Inception: Usage, Trends, and Potential. *Remote Sens.* **2018**, *10*, 1509. [[CrossRef](#)]

44. Masek, J.G.; Vermote, E.F.; Saleous, N.E.; Wolfe, R.; Hall, F.G.; Huemmrich, K.F.; Gao, F.; Kutler, J.; Lim, T.K. A Landsat surface reflectance dataset for North America, 1990–2000. *IEEE Geosci. Remote Sens. Lett.* **2006**, *3*, 68–72. [[CrossRef](#)]
45. Vermote, E.; Justice, C.; Claverie, M.; Franch, B. Preliminary analysis of the performance of the Landsat 8/OLI land surface reflectance product. *Remote Sens. Environ.* **2016**, *185*, 46–56. [[CrossRef](#)]
46. Foga, S.; Scaramuzza, P.L.; Guo, S.; Zhu, Z.; Dilley, R.D.; Beckmann, T.; Schmidt, G.L.; Dwyer, J.L.; Hughes, M.J.; Laue, B. Cloud detection algorithm comparison and validation for operational Landsat data products. *Remote Sens. Environ.* **2017**, *194*, 379–390. [[CrossRef](#)]
47. Goulden, M.L.; Bales, R.C. California forest die-off linked to multi-year deep soil drying in 2012–2015 drought. *Nat. Geosci.* **2019**, *12*, 632–637. [[CrossRef](#)]
48. Flood, N. Continuity of Reflectance Data between Landsat-7 ETM+ and Landsat-8 OLI, for Both Top-of-Atmosphere and Surface Reflectance: A Study in the Australian Landscape. *Remote Sens.* **2014**, *6*, 7952–7970. [[CrossRef](#)]
49. He, T.; Liang, S.L.; Wang, D.D.; Cao, Y.F.; Gao, F.; Yu, Y.Y.; Feng, M. Evaluating land surface albedo estimation from Landsat MSS, TM, ETM plus, and OLI data based on the unified direct estimation approach. *Remote Sens. Environ.* **2018**, *204*, 181–196. [[CrossRef](#)]
50. Roy, D.P.; Kovalsky, V.; Zhang, H.K.; Vermote, E.F.; Yan, L.; Kumar, S.S.; Egorov, A. Characterization of Landsat-7 to Landsat-8 reflective wavelength and normalized difference vegetation index continuity. *Remote Sens. Environ.* **2016**, *185*, 57–70. [[CrossRef](#)]
51. Cohen, W.B.; Yang, Z.Q.; Heale, S.P.; Kennedy, R.E.; Gorelic, N. A LandTrendr multispectral ensemble for forest disturbance detection. *Remote Sens. Environ.* **2018**, *205*, 131–140. [[CrossRef](#)]
52. Guo, J.; Gong, P. The Potential of Spectral Indices in Detecting Various Stages of Afforestation over the Loess Plateau Region of China. *Remote Sens.* **2018**, *10*, 1492. [[CrossRef](#)]
53. Yang, J.; Huang, X. The 30 m annual land cover dataset and its dynamics in China from 1990 to 2019. *Earth Syst. Sci. Data* **2021**, *13*, 3907–3925. [[CrossRef](#)]
54. Li, C.C.; Wang, J.; Hu, L.Y.; Yu, L.; Clinton, N.; Huang, H.B.; Yang, J.; Gong, P. A Circa 2010 Thirty Meter Resolution Forest Map for China. *Remote Sens.* **2014**, *6*, 5325–5343. [[CrossRef](#)]
55. Potapov, P.; Li, X.Y.; Hernandez-Serna, A.; Tyukavina, A.; Hansen, M.C.; Kommareddy, A.; Pickens, A.; Turubanova, S.; Tang, H.; Silva, C.E.; et al. Mapping global forest canopy height through integration of GEDI and Landsat data. *Remote Sens. Environ.* **2021**, *253*, 112165. [[CrossRef](#)]
56. Kennedy, R.E.; Yang, Z.Q.; Gorelick, N.; Braaten, J.; Cavalcante, L.; Cohen, W.B.; Healey, S. Implementation of the LandTrendr Algorithm on Google Earth Engine. *Remote Sens.* **2018**, *10*, 691. [[CrossRef](#)]
57. de Jong, S.M.; Shen, Y.C.; de Vries, J.; Bijnaar, G.; van Maanen, B.; Augustinus, P.; Verweij, P. Mapping mangrove dynamics and colonization patterns at the Suriname coast using historic satellite data and the LandTrendr algorithm. *Int. J. Appl. Earth Obs.* **2021**, *97*, 102293. [[CrossRef](#)]
58. Du, Z.R.; Yu, L.; Yang, J.Y.; Xu, Y.D.; Chen, B.; Peng, S.S.; Zhang, T.T.; Fu, H.H.; Harris, N.; Gong, P. A global map of planting years of plantations. *Sci. Data* **2022**, *9*, 141. [[CrossRef](#)]
59. Yu, L.; Wang, J.; Li, X.; Li, C.; Zhao, Y.; Gong, P. A multi-resolution global land cover dataset through multisource data aggregation. *Sci. China Earth Sci.* **2014**, *57*, 2317–2329. [[CrossRef](#)]
60. Liu, C.; Wang, S.; Liu, H.; Zhu, W.Q. Why did the 1980s’ reform of collective forestland tenure in southern China fail? *Forest Policy Econ.* **2017**, *83*, 131–141. [[CrossRef](#)]
61. Xian, Y.Y.; Lu, Y.Q.; Musyimi, Z.; Liu, G.L. Tracking the Role of Policies and Economic Factors in Driving the Forest Change Trajectories within the Guangdong-Hongkong-Macao Region of China: A Remote Sensing Perspective. *Land* **2021**, *10*, 87. [[CrossRef](#)]
62. Wei, X. Current situation and problems of fast-growing and high-yielding plantation in China. *For. Inventory Plan.* **2021**, *35*, 115–118.
63. Xiao, J.F. Satellite evidence for significant biophysical consequences of the “Grain for Green” Program on the Loess Plateau in China. *J. Geophys. Res. Biogeosci.* **2014**, *119*, 2261–2275. [[CrossRef](#)]
64. Cao, S.X.; Chen, L.; Liu, Z.D. An Investigation of Chinese Attitudes toward the Environment: Case Study Using the Grain for Green Project. *Ambio* **2009**, *38*, 55–64. [[CrossRef](#)] [[PubMed](#)]
65. Yang, X.H.; Zhao, Y.C.; Zhu, S.W.; Yang, X.T.; Wang, L.Y.; Li, Z.Q.; Liu, Z.H.; Yang, S.L.; Xiong, D.G.; Wang, G.X.; et al. *Guangdong Statistical Yearbook*; Guangdong Yearbook Press: Guangdong, China, 2021.
66. Pan, Y.; Chen, J.M.; Birdsey, R.; McCullough, K.; He, L.; Deng, F. Age structure and disturbance legacy of North American forests. *Biogeosciences* **2011**, *8*, 715–732. [[CrossRef](#)]
67. Senf, C.; Lastovicka, J.; Okujeni, A.; Heurich, M.; van der Linden, S. A generalized regression-based unmixing model for mapping forest cover fractions throughout three decades of Landsat data. *Remote Sens. Environ.* **2020**, *240*, 111691. [[CrossRef](#)]
68. Zhu, Z.; Woodcock, C.E. Object-based cloud and cloud shadow detection in Landsat imagery. *Remote Sens. Environ.* **2012**, *118*, 83–94. [[CrossRef](#)]
69. Simard, M.; Pinto, N.; Fisher, J.B.; Baccini, A. Mapping forest canopy height globally with spaceborne lidar. *J. Geophys. Res.-Biogeosci.* **2011**, *116*, G04021. [[CrossRef](#)]

**Disclaimer/Publisher’s Note:** The statements, opinions and data contained in all publications are solely those of the individual author(s) and contributor(s) and not of MDPI and/or the editor(s). MDPI and/or the editor(s) disclaim responsibility for any injury to people or property resulting from any ideas, methods, instructions or products referred to in the content.